ChemComm

COMMUNICATION

Cite this: *Chem. Commun.*, 2022, **58**, 5785

Received 13th February 2022,
Accepted 4th April 2022

DOI: 10.1039/d2cc00891b

rsc.li/chemcomm

Unexpected structures of the Au_{17} gold cluster: the stars are shining†

Pham Vu Nhat, *[a] Nguyen Thanh Si, [a] Vitaly G. Kiselev, [bc] André Fielicke, [d] Hung Tan Pham [e] and Minh Tho Nguyen *[f]

The Au_{17} gold cluster was experimentally produced in the gas phase and characterized by its vibrational spectrum recorded using far-IR multiple photon dissociation (FIR-MPD) of $Au_{17}Kr$. DFT and coupled-cluster theory PNO-LCCSD(T)-F12 computations reveal that, at odds with most previous reports, Au_{17} prefers two star-like forms derived from a pentaprism added by two extra Au atoms on both top and bottom surfaces of the pentaprism, along with five other Au atoms each attached on a lateral face. A good agreement between calculated and FIR-MPD spectra indicates a predominant presence of these star-like isomers. Stabilization of a star form arises from strong orbital interactions of an Au_{12} core with a five-Au-atom string.

Owing to their particular properties and numerous applications in devices with nanoscale dimensions,[1–3] such as chemical/biological sensors,[4] in biomedical sciences[5] and catalysis,[6–8] gold clusters are among the most characterized transition metal nanoparticles to date.[9] As a result of the strong relativistic effect of the element gold,[10–12] small pure Au_n clusters prefer a planar or quasi-planar shape, and a structural transition going from a two-dimensional (2D) to a three-dimensional (3D) configuration takes place at the sizes n = 8–13 depending on their charge states,[13–16] whereas larger systems from n = 16–18 tend to exist as hollow cages.[17,18] Some of us[19] demonstrated a plausible coexistence of both planar and non-planar isomers of Au_{10} at the onset of a 2D–3D structural transition of neutral gold clusters. Since an experimental evidence for hollow golden cages was reported for the Au_{16}^- and Au_{17}^- anions,[17,20] several studies have been devoted to the structures and properties of these sizes. Such golden cages can also trap a foreign atom resulting in a new category of encapsulated golden cage.[21] Although several large golden cages were theoretically predicted,[21–23] none of them has been observed experimentally yet.

Here we will focus on the pure and neutral Au_{17} cluster. Fig. S1 of the ESI† file gives a summary of the structures previously assigned as the most stable form of Au_{17}.[17–26] They were obtained using different functionals (DFT) and differ greatly from each other.[17–26] While a hollow cage **17_3** (*cf.* Fig. 1) was predicted as a ground state,[17,24] a distorted tetrahedral D_{2d} shape **17_6** resulting from a T_d structure of Au_{17}^+ was also

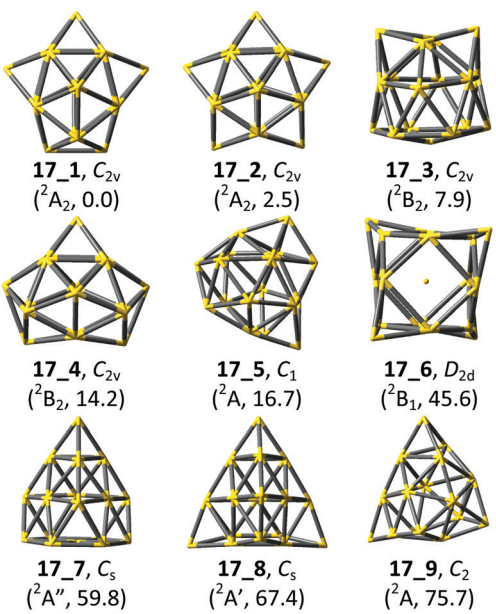

Fig. 1 Some low-lying Au_{17} isomers along with their symmetry point groups and relative energies with respect to the lowest-lying isomer **17_1** (kJ mol^{-1} obtained from PNO-LCCSD(T)-F12b/aug-cc-pVDZ-PP + ZPE computations).

[a] *Department of Chemistry, Can Tho University, Can Tho, Vietnam*
[b] *Novosibirsk State University, 1 Pirogova Str., 630090 Novosibirsk, Russia*
[c] *Institute of Chemical Kinetics and Combustion SB RAS, 3 Institutskaya Str., 630090 Novosibirsk, Russia*
[d] *Fritz-Haber-Institut der Max-Planck-Gesellschaft, Faradayweg 4–6, 14195 Berlin, Germany*
[e] *Department of Chemistry, KU Leuven, Celestijnenlaan 200F, 3001 Leuven, Belgium*
[f] *Institute for Computational Science and Technology (ICST), Ho Chi Minh City, Vietnam. E-mail: tho.nm@icst.org.vn*

† Electronic supplementary information (ESI) available. See DOI: https://doi.org/10.1039/d2cc00891b

suggested.[25] However, a new putative ground state structure, *i.e.* **17_7** (Fig. 1), is not consistent with all those proposed earlier. Recently some of us[19] found a star-like structure (**17_2** in Fig. 1) but such a prediction was not certain because it was based on the energies obtained with one particular DFT functional.

In view of such a discrepancy, we set out to perform a combined experimental and theoretical study to revisit the Au_{17} structure. From extensive geometry searches, we find two new structural motifs for this size that have been overlooked in the literature, and both are found to be more stable than those previously reported (Fig. S1, ESI†).

Quantum chemical results presented hereafter are determined using a range of DFT[27–31] and wavefunction theory (coupled-cluster theory)[32–34] methods that are described in the ESI† file along with details on the IR-MPD experiment.

The shapes of the low-lying Au_{17} isomers along with their symmetry point groups and relative energies are shown in Fig. 1, while their Cartesian coordinates are given in Table S1 of the ESI† file. Previous structures given in Fig. S1 (ESI†) are also labeled following those in Fig. 1. In recent calculations[26,35] using both PW91 and BB95 functionals, the C_s **17_7** (Fig. 1) which is obtained upon removal of three corner Au atoms from the Au_{20} tetrahedron[35] was reported as the Au_{17} global energy minimum. This is not consistent with a previous result using the TPSS functional[25] which yields D_{2d} **17_6**. The latter can be constructed by adding four Au atoms on an fcc octahedral core of Au_{13}. On the contrary, earlier calculations[36,37] using the PBE functional predicted the C_{2v} hollow cage **17_3**, as in the Au_{17}^- anion.[17]

Almost all DFT results, and more importantly the coupled-cluster PNO-LCCSD(T)-F12 results, obtained in the present work predict both star-like cage structures **17_1** and **17_2** to be the most stable isomers of Au_{17} (Fig. 1, Table 1). Both star forms are basically degenerate in energy and can be built from an Au_{10} pentaprism followed by addition of two extra Au atoms on both top and bottom surfaces of the pentaprism, along with attachment of five other Au atoms, each on a lateral face. The main difference between them is that while two of the latter atoms form a bond in **17_1**, they are separated in **17_2**. The most striking finding is that these star-like **17_1** motifs which has been overlooked in previous reports (Fig. S1, ESI†) could emerge as the lowest-lying isomers of Au_{17}.

Table 1 Relative energies ΔE (kJ mol^{-1}) of low-lying Au_{17} isomers computed using different methods (VnZ stands for cc-pVnZ and a for augmented)

	TPSS	revTPSS	PBE	PW91	M06	PNO-LCCSD(T)-F12b	
Isomer	VDZ-PP					aVDZ-PP	aVTZ-PP
17_1	2.5	2.9	0.0	0.0	0.0	0.0	0.0
17_2	0.0	0.0	0.0	0.2	3.8	2.5	5.0
17_3	4.2	1.7	3.3	2.9	5.4	7.9	7.1
17_4	10.5	5.9	7.1	9.6	8.8	14.2	15.5
17_5	11.7	10.0	11.7	11.7	14.6	16.7	17.2
17_6	2.9	7.9	21.8	28.0	46.0	45.6	45.6
17_7	19.7	9.6	36.0	36.4	41.8	59.8	—
17_8	19.2	18.0	38.5	41.0	71.1	67.4	—
17_9	33.9	31.4	42.3	43.5	58.2	75.7	—

For better visualization, Fig. S2 (ESI†) displays the shapes of both star forms in different perspectives. The **17_1**, **17_2**, **17_3** and **17_4** isomers displayed in Fig. 1 are slightly distorted to a C_{2v}, instead of adopting D_{5h} group as in a regular pentaprism, due to a Jahn–Teller effect on their open-shell electronic structure. More specifically, the single occupancy of one doubly degenerate orbital e_1'' of a D_{5h} structure invariably leads to a geometric change giving rise to an orbital splitting to a pair of (a_2 + b_2) orbitals in a C_{2v} form. The unpaired electron in the C_{2v} **17_1** occupies the a_2 SOMO (Fig. S3, ESI†), resulting in a $^2A_2$ state. The **17_3** is the $^2B_2$ component of the splitting pair, lying $\sim$7 kJ mol^{-1} higher. Similarly, both C_{2v} **17_2** and **17_4** isomers are formed from a splitting of the second e_1'' orbital giving another (a_2 + b_2) pair following geometry relaxation in a different direction. The energy difference between the latter pair of isomers amounts to 10 kJ mol^{-1} (Table 1).

While both $^2A_2$ states keep a star-like shape, both $^2B_2$ components have substantially modified geometries. According to DFT results, both star-like structures **17_1** and **17_2** are strongly competing with each other to be the Au_{17} ground state. The TPSS functional predicts **17_2** to be slightly favoured over **17_1** by 2.5 kJ mol^{-1} (Table 1). Nonetheless, calculations using another density functional may result in a different potential energy surface topology, as the energy ordering of isomers is known to be quite sensitive with respect to the density functional employed.[31,38,39] In fact, while revTPSS and PBE functionals assign **17_2** as the global minimum, PW91 and M06 predict **17_1** to be more stable, always with a small energy gap of $<$4 kJ mol^{-1}. None of the functionals employed here results in **17_3**, **17_6**, **17_7** or **17_8** to be the lowest-lying isomer as previously reported (*cf.* Fig. S1, ESI†).

In this context, we perform single-point electronic energy calculations for low-lying Au_{17} isomers using the novel local modifications of the explicitly correlated coupled-cluster theory PNO-LCCSD(T)-F12. In terms of both accuracy and cost, the latter yields results in reasonable agreement with the conventional CCSD(T) values.[40,41] Very often, even a double-zeta basis set is sufficient for attaining the chemical accuracy of $\pm$4 kJ mol^{-1}.[42–44] To stay on a safe side, we further compute PNO-LCCSD(T)-F12 relative energies of **17_1**–**17_6** isomers with the larger aug-cc-pVTZ-PP basis set. We find that the largest discrepancy between both DZ and TZ basis sets is $<$2.5 kJ mol^{-1} (Table 1).

PNO-LCCSD(T)-F12 results again confirm that both **17_1** and **17_2** (*cf.* Fig. 1), being within an energy difference of $\sim$5 kJ mol^{-1}, are the most energetically preferable isomers of Au_{17}. In agreement with PW91 and M06 predictions, **17_1** is slightly more energetically favourable whereas **17_6** becomes much less stable with a PNO-LCCSD(T)-F12 relative energy of $\sim$46 kJ mol^{-1}. **17_3**, **17_4** and **17_5** lie also close to the global minimum **17_1** (within $\sim$17 kJ mol^{-1}). **17_7**, **17_8** and **17_9** are much less stable, being 60 kJ mol^{-1} higher in energy. Both **17_6** and **17_7** were reported to be the putative global minima in previous computations (Fig. S1, ESI†).[12,25,45] The present high accuracy results do not support such assignments.

In terms of free energies (ΔG), when using DFT (TPSS and revTPSS) results, **17_2** remains more stable than **17_1** by

2.1 kJ mol^{-1} at 100 K, 3.3 kJ mol^{-1} at 200 K, and both practically have the same free energy at 300 K. Otherwise noted, the free energy ordering follows that of the corresponding enthalpy. Overall, in view of the small energy difference between both star-like isomers **17_1** and **17_2** whose ordering is interchanged with respect to the method employed, both in terms of enthalpy and free energy, we would conclude that they are basically quasi-degenerate in energy.

The high thermodynamic stability of both star-like forms can be understood by orbital interactions. Let us consider **17_2** whose electronic structure can be analyzed by constructing orbital interactions between an inner Au_{12} core containing a pentaprism and an outer Au_5 string. The resulting correlation diagram built up under a C_{2v} point group is illustrated in Fig. S4 (ESI†) which also displays the main shell orbitals.

Such a core structure does not correspond to the lowest-lying form of Au_{12} and lies much higher in energy than its global minimum. The five Au atoms of the outer string are located far away from each other, and do no interact with each other, and for the sake of simplicity, their 6s-MO are omitted in Fig. S4 (ESI† file). It is clear that the MOs of the C_{2v} Au_{12} core are strongly stabilized upon interaction, and thereby lead to a low-energy **17_2**. A similar orbital interaction feature can also be established for the distorted star form **17_1**.

The total density of states (DOS) and some shell orbitals of **17_2** are displayed in Fig. 2. Accordingly, the 17 valence electrons of the Au_{17} radical occupy a nearly closed electron shell of the [1S^2 1P^6 1D^9] configuration.

Both the experimental and simulated IR spectra for the low-lying Au_{17} structures are shown in Fig. 3. Although complexation with the messenger Kr atoms may have a certain influence on the isomer distribution and appearance of IR spectra, the comparably weak interactions between krypton atoms and the neutral gold clusters is expected to induce very small effects on the IR spectra.[46]

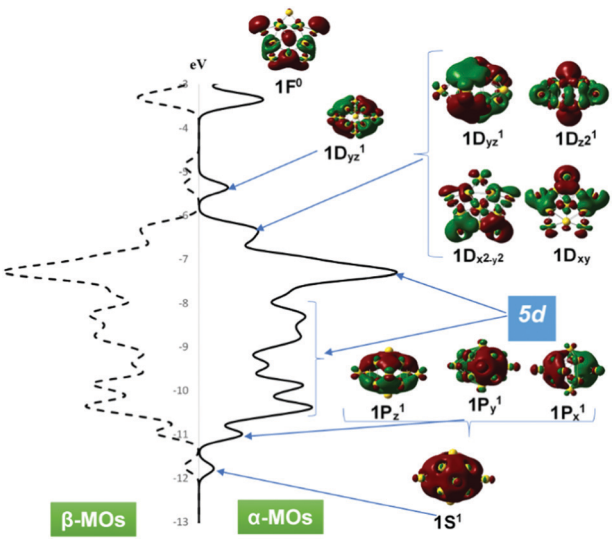

Fig. 2 Density of states (DOS) and some shell orbitals of Au_{17} **17_2**.

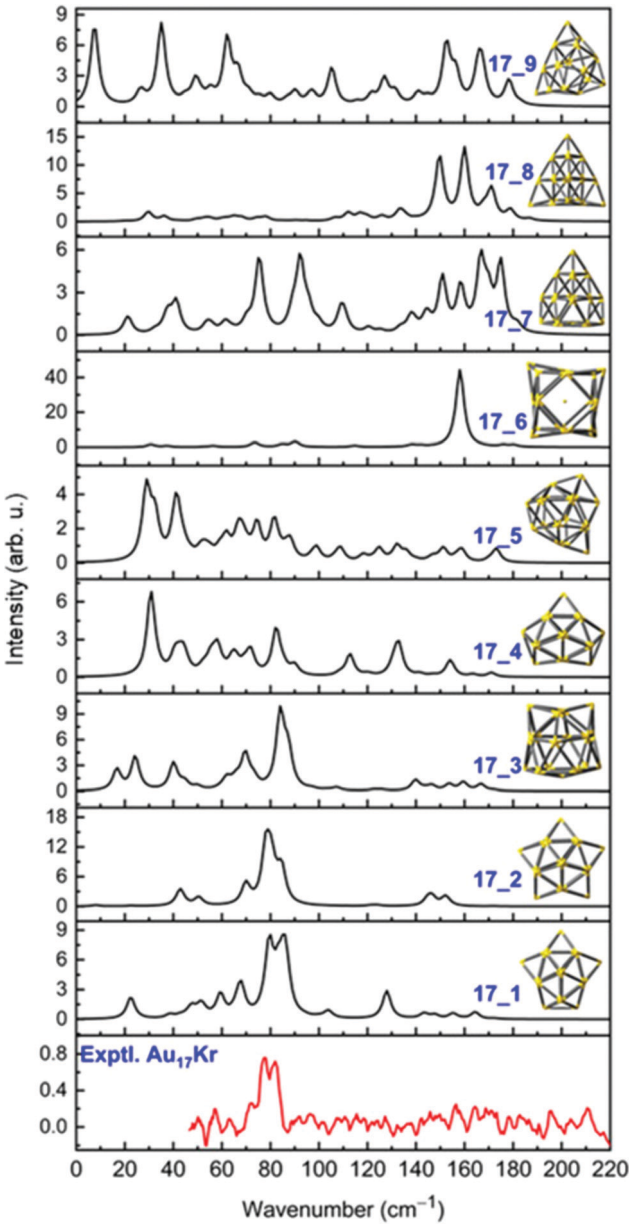

Fig. 3 Experimental FIR-MPD of Au_{17}–Kr and theoretical IR spectra of Au_{17}. Simulations are made using harmonic vibrational frequencies (without scaling) and intensities obtained by revTPSS/cc-pVDZ-PP computations.

As compared to other neutral Au_n clusters,[47,48] the IR spectrum of Au_{17} is rather specific with the absence of prominent bands above 100 cm^{-1}. The experimental FIR-MPD spectrum is dominated by a single broad peak centered at ~80 cm^{-1}. The predicted IR spectra of both isomers **17_1** and **17_2** are also characterized by having their most intense feature centered at 80–90 cm^{-1}, arising in each case from several overlapping absorptions. They show additional lines near 60 cm^{-1}, for which **17_1** gives a slightly better match to the experimental spectrum. Overall, both isomers **17_1** and **17_2** can well be assigned to the experimental FIR-MPD spectrum of $Au_{17}Kr$ (Fig. 3). The spectrum of **17_3** exhibits a less good

match to the experimental as compared to **17_1** and **17_2**, but its contribution cannot be ruled out entirely. On the contrary, the simulated IR spectra of higher-lying isomers, *i.e.* from **17_4** to **17_9**, typically miss the prominent signal at $\sim$80 cm^{-1} but instead contain intense bands at above 100 cm^{-1}. They clearly do not match the experiment (Fig. 3). Because both **17_1** and **17_2** are energetically quasi-degenerate, and their IR spectra are very similar to each other, they, either just a single isomer or a mixture of both, likely contribute to the observed FIR-MPD spectrum of $Au_{17}Kr$. Normal coordinates of the active vibrational modes of **17_1** and **17_2** are displayed in the TOC Graphic.

In summary, by a combination of far-infrared multiple photon dissociation spectroscopy and extensive computations using DFT and wavefunction methods, structures for the neutral Au_{17} cluster were assigned. Two new stable isomers, both having a distorted star-like shape and containing a core pentaprism capped with seven Au atoms placed outside, were identified. Formation of such golden stars is intriguing as it has never been detected before for neutral gold or other coinage metal clusters. Their vibrational signatures are characterized by stretching of bonds linked to the inner pentaprism that results in prominent peaks centered at $\sim$80 cm^{-1}.

Experiment and computation: details and references are given in the (ESI†) file.

This work is funded by VinGroup (Vietnam) and supported by VinGroup Innovation Foundation (VinIF) under project code VinIF.2020.DA21.

AF thanks G. Meijer for his continuing support and gratefully acknowledges the Stichting voor Fundamenteel Onderzoek der Materie (FOM) in providing beam time on FELIX, the skillful assistance of the FELIX staff, and the contributions of his co-authors of ref. 46–48 for obtaining the experimental data.

Conflicts of interest

The authors declare no competing financial interest.

References

1 H. Zhang, G. Schmid and U. Hartmann, *Nano Lett.*, 2003, **3**, 305–307.
2 M. C. Daniel and D. Astruc, *Chem. Rev.*, 2004, **104**, 293–346.
3 P. Schwerdtfeger, *Angew. Chem., Int. Ed.*, 2003, **42**, 1892–1895.
4 K. Saha, S. S. Agasti, C. Kim, X. Li and V. M. Rotello, *Chem. Rev.*, 2012, **112**, 2739–2779.
5 L. A. Austin, M. A. Mackey, E. C. Dreaden and M. A. El-Sayed, *Arch. Toxicol.*, 2014, **88**, 1391–1417.
6 J. H. Teles, S. Brode and M. Chabanas, *Angew. Chem., Int. Ed.*, 1998, **37**, 1415–1418.
7 R. M. Veenboer, S. Dupuy and S. P. Nolan, *ACS Catal.*, 2015, **5**, 1330–1334.
8 M. Rudolph and A. S. K. Hashmi, *Chem. Commun.*, 2011, **47**, 6536–6544.
9 P. V. Nhat, N. T. Si, N. T. T. Tram, L. V. Duong and M. T. Nguyen, *J. Comput. Chem*, 2020, **41**, 1748–1758.
10 P. Pyykko, *Chem. Rev.*, 1988, **88**, 563–594.
11 P. Schwerdtfeger, M. Dolg, W. H. E. Schwarz, G. A. Bowmaker and P. D. W. Boyd, *J. Chem. Phys.*, 1989, **91**, 1762–1774.
12 B. Assadollahzadeh and P. Schwerdtfeger, *J. Chem. Phys.*, 2009, **131**, 064306.
13 M. P. Johansson, I. Warnke, A. Le and F. Furche, *J. Phys. Chem. C*, 2014, **118**, 29370–29377.
14 P. Pyykkö, *Chem. Rev. Soc.*, 2008, **37**, 1967–1997.
15 M. Gruber, G. Heimel, L. Romaner, J.-L. Brédas and E. Zojer, *Phys. Rev. B: Condens. Matter Mater. Phys.*, 2008, **77**, 165411.
16 P. V. Nhat, N. T. Si, N. T. N. Hang and M. T. Nguyen, *Phys. Chem. Chem. Phys.*, 2022, **24**, 42–47.
17 S. Bulusu, X. Li, L.-S. Wang and X. C. Zeng, *Proc. Natl. Acad. Sci. U. S. A.*, 2006, **103**, 8326–8330.
18 W. Huang, S. Bulusu, R. Pal, X. C. Zeng and L.-S. Wang, *ACS Nano*, 2009, **3**, 1225–1230.
19 N. H. Tho, T. Q. Bui, N. T. Si, P. V. Nhat and N. T. A. Nhung, *J. Mol. Mod.*, 2022, **28**, 54–64.
20 X. Xing, B. Yoon, U. Landman and J. H. Parks, *Phys. Rev. B: Condens. Matter Mater. Phys.*, 2006, **74**, 165423.
21 X. Gu, M. Ji, S. Wei and X. Gong, *Phys. Rev. B: Condens. Matter Mater. Phys.*, 2004, **70**, 205401.
22 L. Trombach, S. Rampino, L. S. Wang and P. Schwerdtfeger, *Chem. – Eur. J.*, 2016, **22**, 8823–8834.
23 Y. Gao and X. C. Zeng, *J. Am. Chem. Soc.*, 2005, **127**, 3698–3699.
24 C. Tang, W. Zhu, K. Zhang, X. He and F. Zhu, *Comput. Theor. Chem.*, 2014, **1049**, 62–66.
25 L. Yan, L. Cheng and J. Yang, *J. Phys. Chem. C*, 2015, **119**, 23274–23278.
26 S. Li, S. Singh, J. A. Dumesic and M. Mavrikakis, *Catal. Sci. Technol.*, 2019, **9**, 2836–2848.
27 J. P. Perdew and Y. Wang, *Phys. Rev. B: Condens. Matter Mater. Phys.*, 1992, **45**, 13244–13249.
28 J. P. Perdew, K. Burke and M. Ernzerhof, *Phys. Rev. Lett.*, 1996, **77**, 3865.
29 J. Tao, J. P. Perdew, V. N. Staroverov and G. E. Scuseria, *Phys. Rev. Lett.*, 2003, **91**, 146401.
30 Y. Zhao and D. G. Truhlar, *Theor. Chem. Acc.*, 2008, **120**, 215–241.
31 J. P. Perdew, A. Ruzsinszky, G. I. Csonka, L. A. Constantin and J. Sun, *Phys. Rev. Lett.*, 2009, **103**, 026403.
32 H. J. Werner, P. J. Knowles, G. Knizia, F. R. Manby and M. Schütz, *Wiley Interdiscip. Rev.: Comput. Mol. Sci.*, 2012, **2**, 242–253.
33 Q. Ma and H.-J. Werner, *J. Chem. Theory Comput.*, 2018, **14**, 198–215.
34 H.-J. Werner, P. J. Knowles, F. R. Manby, J. A. Black, K. Doll, A. Heßelmann, D. Kats, A. Köhn, T. Korona and D. A. Kreplin, *J. Chem. Phys.*, 2020, **152**, 144107.
35 P. V. Nhat, N. T. Si, J. Leszczynski and M. T. Nguyen, *Chem. Phys.*, 2017, **493**, 140–148.
36 S. Bulusu and X. C. Zeng, *J. Chem. Phys.*, 2006, **125**, 154303.
37 A. Yang, W. Fa and J. Dong, *Phys. Lett. A*, 2010, **374**, 4506–4511.
38 P. V. Nhat, N. T. Si and M. T. Nguyen, *J. Phys. Chem. A*, 2020, **124**, 1289–1299.
39 D. A. Götz, R. Schäfer and P. Schwerdtfeger, *J. Comput. Chem.*, 2013, **34**, 1975–1981.
40 L. Kong, F. A. Bischoff and E. F. Valeev, *Chem. Rev.*, 2012, **112**, 75–107.
41 Q. Ma and H.-J. Werner, *J. Chem. Theory Comput.*, 2019, **15**, 1044–1052.
42 V. G. Kiselev, *Phys. Chem. Chem. Phys.*, 2015, **17**, 10283–10284.
43 V. G. Kiselev and C. F. Goldsmith, *J. Phys. Chem. A*, 2019, **123**, 4883–4890.
44 M. V. Gorn, N. P. Gritsan, C. F. Goldsmith and V. G. Kiselev, *J. Phys. Chem. A*, 2020, **124**, 7665–7677.
45 R. R. Persaud, M. Chen and D. A. Dixon, *J. Phys. Chem. A*, 2020, **124**, 1775–1786.
46 L. M. Ghiringhelli, P. Gruene, J. T. Lyon, D. M. Rayner, G. Meijer, A. Fielicke and M. Scheffler, *New J. Phys.*, 2013, **15**, 083003.
47 P. Gruene, D. M. Rayner, B. Redlich, A. F. van der Meer, J. T. Lyon, G. Meijer and A. Fielicke, *Science*, 2008, **321**, 674–676.
48 B. R. Goldsmith, J. Florian, J.-X. Liu, P. Gruene, J. T. Lyon, D. M. Rayner, A. Fielicke, M. Scheffler and L. M. Ghiringhelli, *Phys. Rev. Mater.*, 2019, **3**, 016002.

